ResearchGate

See discussions, stats, and author profiles for this publication at: https://www.researchgate.net/publication/47508850

Spirooxazine to Merooxazine Interconversion in the Presence and Absence of Zinc: Approach to a Bistable Photochemical Switch

ARTICLE *in* THE JOURNAL OF PHYSICAL CHEMISTRY A · OCTOBER 2010

Impact Factor: 2.69 · DOI: 10.1021/jp106501e · Source: PubMed

CITATIONS
14

READS
12

7 AUTHORS, INCLUDING:

Robert A Stairs
Trent University
28 PUBLICATIONS **144** CITATIONS
SEE PROFILE

Julian M. Dust
Grenfell Campus-Memorial University of N…
61 PUBLICATIONS **971** CITATIONS
SEE PROFILE

Thomas M Kraft
Tampere University of Technology
9 PUBLICATIONS **59** CITATIONS
SEE PROFILE

Available from: Julian M. Dust
Retrieved on: 24 January 2016

Spirooxazine to Merooxazine Interconversion in the Presence and Absence of Zinc: Approach to a Bistable Photochemical Switch

Zhiyuan Tian,[†] Robert A. Stairs,[‡] Martin Wyer,[†] Nicholas Mosey,[†] Julian M. Dust,[§] Thomas M. Kraft,[†] and Erwin Buncel*,[†]

Department of Chemistry, Queen's University, Kingston, ON. Canada K7L 3N6, Department of Chemistry, Trent University, Peterborough, ON Canada K9J 7B8, and Departments of Chemistry and Environmental Science, Grenfell Campus, Memorial University of Newfoundland, Corner Brook, Newfoundland and Labrador, Canada A2H 6P9

Received: July 13, 2010; Revised Manuscript Received: September 15, 2010

A spironaphthoxazine (SO) photoswitch was synthesized, and its photochromic behaviors were investigated. SO underwent reversible ring-opening/closure isomerization between a spirocyclic isomer (closed form) and a merocyanine (MO isomer, open form) upon ultraviolet light irradiation. For the model SO in this work, the thermal equilibrium is substantially shifted toward the spirocyclic isomer even at −30.0 °C. However, addition of zinc, as $Zn(ClO_4)_2$, exerted an important effect on the thermal reversion process from the open (MO) to the closed form (SO). Kinetic analysis showed that thermal reversion with zinc is retarded more than 13-fold, significantly improving bistability. Moreover, introduction of zinc to the spirooxazine−merooxazine (SO−MO) system resulted in a new absorption band readily distinguishable from the bands arising from spirooxazine and merooxazine. For the first time, to the best of our knowledge, the microscopic rate constants for: MO photogeneration from SO (k_1), thermal reversion of MO to SO (k_2), complexation of MO with zinc (k_3) and for dissociation of the complex, MO−Zn (k_4), as well as for the ionization equilibria of $Zn(ClO_4)_2$ have been evaluated. The preferred transoid structures of MO and those of MO−Zn derived from the preferred MO structures are considered. Although the kinetic study does not permit elucidation of the nature of zinc binding to MO to give MO−Zn, nor the precursor isomers of MO, a DFT calculational study in progress should shed light on the structure and relative stability of these essential intermediates.

Introduction

Tunability is of vital importance in the development of practical molecular photoswitching. Thus, among the properties of thermo- and photochromic dye molecules, tunability toward external stimuli through application of heat and radiation can govern interchangeability between noncolored and colored forms.[1] A prime example is the spiropyran (SP)−merocyanine (MC) system,[2] where UV radiation-induced ring-opening transforms the orthogonal SP to the planar conjugated MC, which is accompanied by change from colorless to purple.[2−4] The reverse ring closure is effected thermally (spontaneously) or through irradiation by visible light.[3] Scheme 1 illustrates SP−MC interconversion for 6′-nitro-1,3,3-trimethylspiro(indolino-2,2′-benzopyran), commonly known as 6-nitro-BIPS.[3−5]

The SP−MC molecular switch has been widely studied because of its potential in imaging, recording, copying, and memory devices.[6] The propensity of MCs for spontaneous reversion to a colorless form results in a distinct drawback to practical utilization. This has led to studies aimed at stabilization of the MC form.[7] To this end, in our laboratory, we have chosen to variously manipulate the system through acid−base equilibria (acidochromic modulation),[8] metal ion coordination to Lewis base centers,[4,9] as well as structural modification (e.g., chelating carboxylate modification).[9−11] We, among other groups,[6d,12] have also been involved in incorporating SP−MC photoswitches into novel media, including liquid crystal phases[13] and most recently as attachments to microparticles.[14]

Among the modes of action that metal ions exhibit in such systems is modulation of the SP−MC reversion via selective metal ion chelation.[9] Here, evidence supports trapping of a *cis*-MC that would otherwise be transient, as illustrated in Figure 1. Schematically, the processes are shown in Scheme 2. Combination of these different stimuli provides avenues for tunability in these photoswitching models.

These stimuli can be extended to analogous structures where kinetic and spectroscopic analysis allows assessment of the degree of control. Thus, structural change of the spiropyrans, where C═CH is replaced by C═N, imparts greater photostability to the resultant spirooxazines (SO).[15] It has been noted that the photochemical fatigue resistance of SO enhances their potential for use in commercial applications.[15c]

In the current study the SO ring also opens upon UV irradiation. A transition state (TS) or intermediate is shown in Scheme 3, where the tetrahedral spiro carbon to oxygen (C−O) bond is in the process of breaking, and these C- and O-centers bear appreciable positive and negative charge, respectively. In polar aprotic solvents, including acetone used here, a fluorescence emission is found that has been attributed to an intermediate cisoid structure similar to the TS of Scheme 3; here the C- and O-centers would bear full positive and negative charges.[16] Completion of ring-opening leads to the merocyanine form(s) (i.e., MO) of which the lowest energy structure, according to calculation,[17] is shown in Scheme 3. Once formed, MO undergoes thermal reversion back to the closed form, SO.

* To whom correspondence should be addressed. E-mail: buncele@chem.queensu.ca.
[†] Queen's University.
[‡] Trent University.
[§] Memorial University of Newfoundland.

10.1021/jp106501e © 2010 American Chemical Society
Published on Web 10/20/2010

SCHEME 1: SP−MC Interconversion for 6-Nitro-BIPS

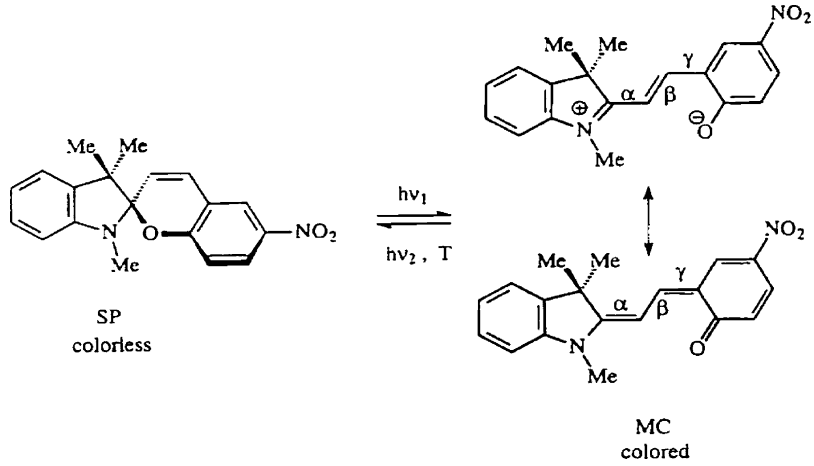

Building upon our understanding of the effects of divalent metal ions in comparable SP−MC systems, we have chosen to examine these effects on the extension of MO lifetime in the current SO−MO system using zinc (as $Zn(ClO_4)_2$ in acetone). The kinetics and effect on MO lifetime that accrues from Zn coordination to MO (i.e., formation of MO−Zn complex) were determined, and insights from statistical treatment and UV−vis spectroscopic deconvolution are discussed. The preferred transoid structures of MO and those of MO−Zn derived from the preferred MO structures are considered.

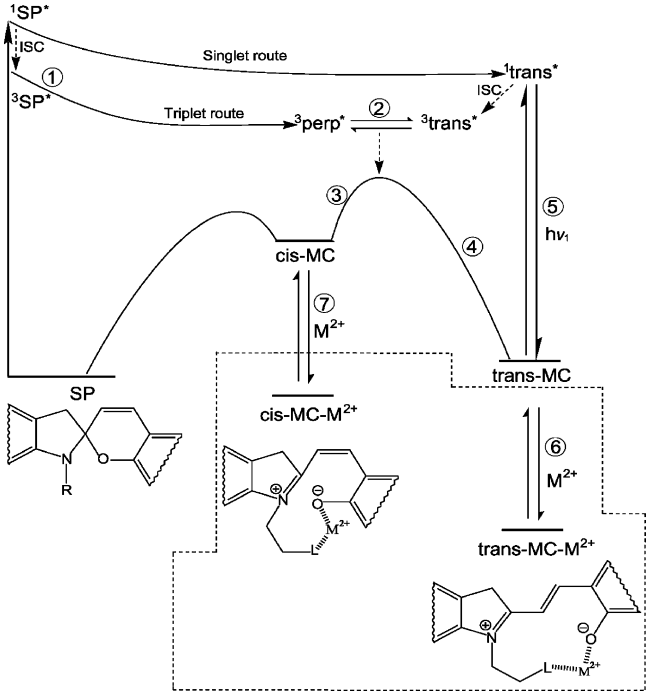

Figure 1. General energy-reaction coordinate diagram for the chelation of SPs in the presence of M^{2+}. Irradiation of SP produces the *cis*- and *trans*-MC isomers (steps 1−5), capable of chelation with M^{2+} (steps 6 and 7). Boxed-in portion (dashed) pertains to the processes during irradiation in the presence of metal salts.[9]

SCHEME 2: SP−MC Reversion via Selective Metal Ion Chelation

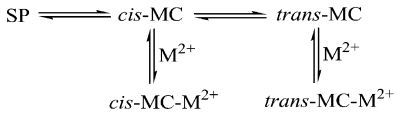

Results and Discussion

1. Overview of SO−MO Interconversion. ***a. In the Absence of Zinc.*** Irradiation of SO (5.5×10^{-5} M, acetone, −30 °C) at 319 nm, where SO absorbs significantly, results in formation of the colored open-form, MO (Scheme 3). A concentration (ca. 5×10^{-5} M) approaching that of the photostationary state is obtained after 300 s of irradiation, at which point the UV−vis spectrum of MO comprises a major peak at 605 nm ($\epsilon_{max} = 45\,000\ M^{-1}\ cm^{-1}$) with a shoulder at 570 nm and smaller bands at 434 and 413 nm. The MO ring closes spontaneously back to the colorless SO form in the dark. This thermal reversion is illustrated spectrally in Figure 2.

As shown in Scheme 3, irradiation of SO at −30 °C in acetone leads to the open MO as described by the rate constant k_1. Irradiation of SO should give an excited state (comparable to that depicted in Figure 1 for SP → MC systems) from which the excited molecule can cross to the transition state (TS) for ring-opening. The TS can be envisaged as cisoid where the spiro C−O bond is elongated and partially broken (Scheme 3, TS). The TS can lead to any of four suggested cisoid forms (not shown) that are presumed transient. Isomerization leads to four, presumably interconvertible, but more stable, transoid forms. Previous gas-phase calculations on the MO formed from SO identified four transoid structures (Scheme 5), labeled CTT, TTT, CTC, and TTC, of which TTC (cf. MO in Scheme 3) was found to be the most stable in the absence of stabilizing metal ions.[17] SO → MO ring-opening is fairly fast ($k(h\nu) = k_1$) under UV irradiation whereas thermal reversion ($k(\Delta) = k_2$) is slower. These kinetic processes will be detailed subsequently. The spectrum and composition of the MO system changes markedly upon the introduction of zinc (as $Zn(ClO_4)_2$), in accord with formation of MO−Zn (Scheme 4).

b. In the Presence of Zinc. Comparable irradiation of SO in the presence of $Zn(ClO_4)_2$ in acetone (ratios of $Zn(ClO_4)_2$:SO of 0.5:1, 1:1, 5:1, 10:1, and 50:1) results in a UV−vis spectrum that retains the prominent 605 nm absorption and the 570 nm shoulder, but these bands are joined by a new peak nominally at 520 nm (Figure 3). The small peaks at 434 and

SCHEME 3: Transition of SO to TTC

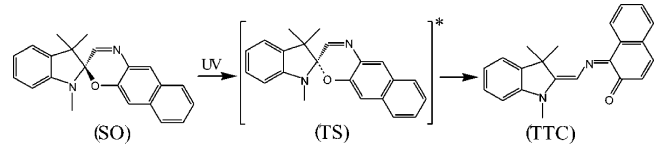

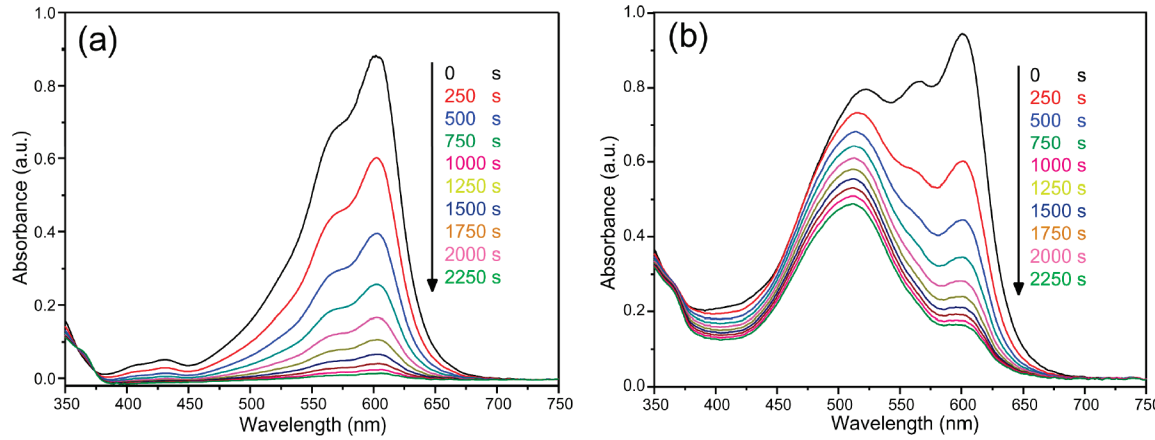

Figure 2. Thermal reversion of MO to SO at −30 °C. UV−vis spectra (300−800 nm) of MO in acetone in the absence (a) and presence (b) of zinc perchlorate at −30 °C: successive scans of absorbance at 250 s intervals from the cessation of irradiation. (a) Zinc absent: peak at 605 with shoulder at ∼570, with small peaks at 434 and 413 nm. (b) In the presence of $Zn(ClO_4)_2$: mole ratio of Zn to total SO + MO concentration 10:1 (i.e., $f = 10$, Figure 5). Additional peak at ∼520 nm due to MO−Zn.

SCHEME 4: Formation of MO−Zn

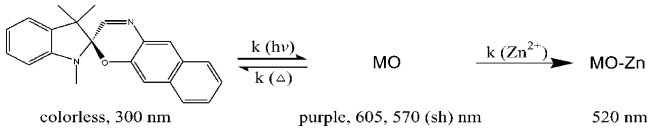

413 nm recorded in the spectrum of MO in the absence of zinc are no longer apparent in the new spectrum where zinc is present (Figure 3). The 520 nm peak provides evidence for the presence of a new species, reasonably incorporating Zn^{2+} with suitable ligands, designated as MO−Zn. Spectra in the presence of

SCHEME 5: Four Transoid Structures of Spironaphthoxazine

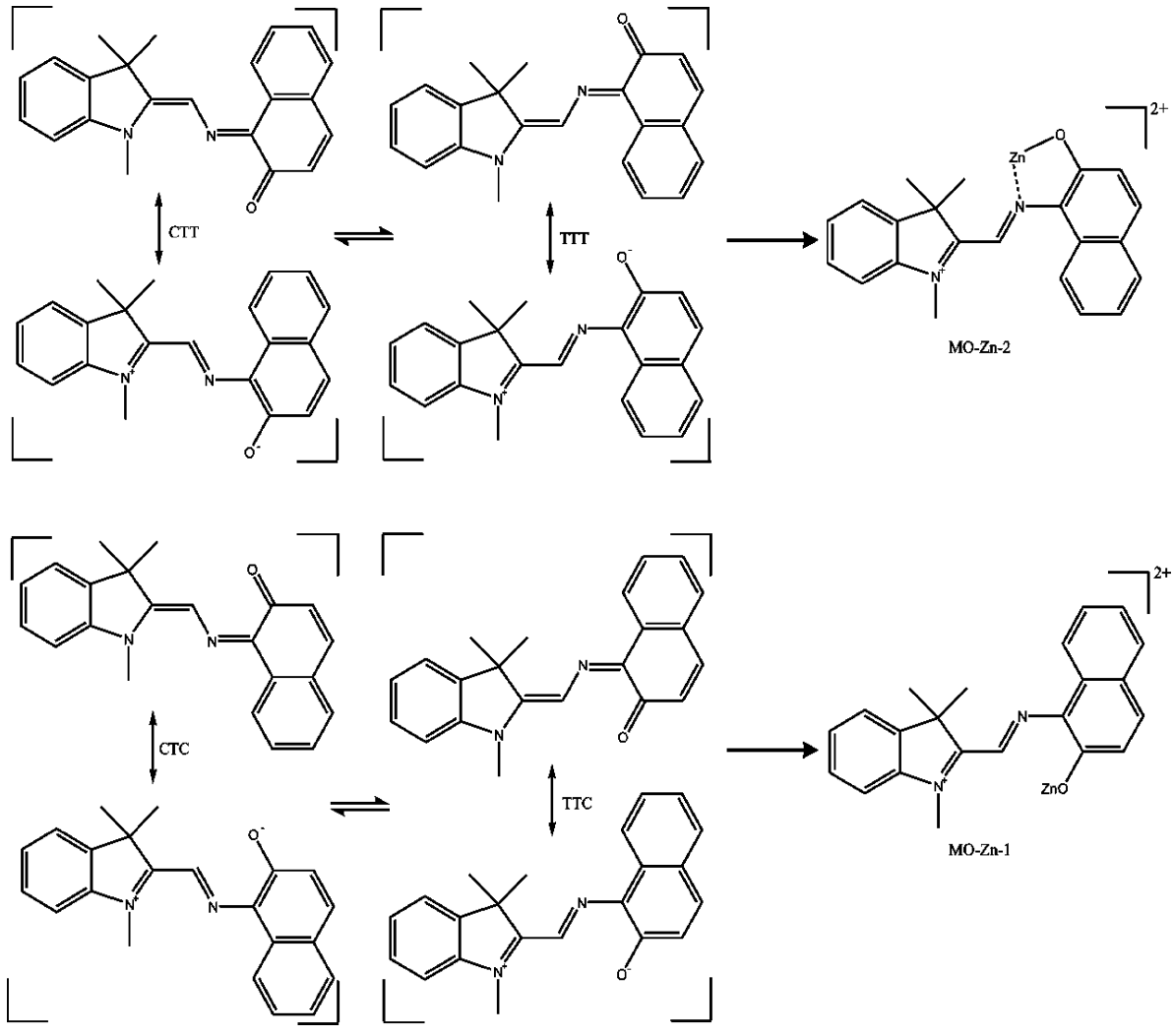

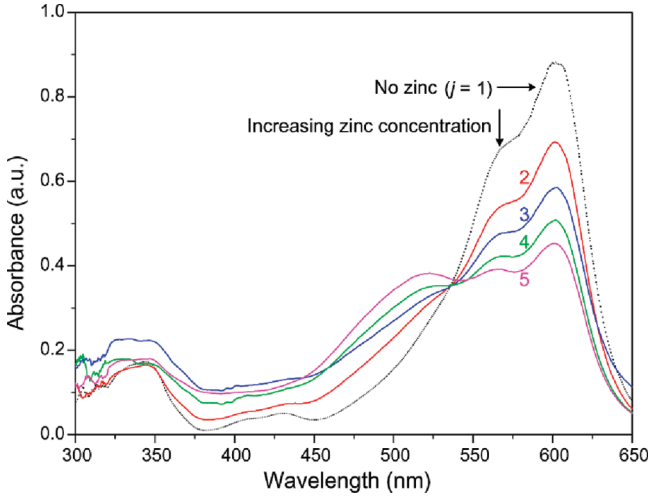

Figure 3. Spectra, taken at approximately the same time in the reaction (ca. 250 s), for varying amounts of added $Zn(ClO_4)_2$. An apparent isosbestic point can be discerned at about 536 nm. Spectra are labeled as $j = 1$ (no added zinc, top spectrum), $j = 2$, ..., 5 with increasing concentrations of $Zn(ClO_4)_2$. (These designations are used in the Deconvolution section.) Note that as the amount of added zinc increases the band at 605 with shoulder at 570 nm for MO declines, while the peak at 520 nm corresponding to MO−Zn increases in intensity.

increasing zinc concentration ratio show that MO undergoes thermal ring closure to colorless SO (Figure 3).

Scheme 4 illustrates the SO → MO photogeneration and MO → SO cyclization processes in the presence of zinc. In this scheme, formation of MO by irradiation of SO leads to one or more MO−zinc complexes, collectively labeled MO−Zn, that is, overall SO + zinc → MO−Zn (presumably via MO structures).

In Scheme 5 we focus on the four transoid structures for MO that have been proposed on the basis of gas-phase calculations.[17] The MO structures represented in Scheme 5 include the charge-separated resonance forms describing each structure (each bracket represents the hybrid of the resonance forms). In a structurally related system, NMR evidence has been reported that also supports the presence of four discrete transoid structures for the comparable MO.[18]

In the absence of metal previous HF ab initio calculations indicate that the TTC form (trans trans cis) is the most stable.[17] On the other hand, it is reasonable to presume that the various forms (CTT, TTT, CTC, and TTC) can equilibrate (as shown by the equilibrium arrows in Scheme 5).[12d] Further, two structures—CTT and TTT—are organized optimally for bidentate complexation of the zinc, whereas the other two structures may reasonably coordinate with zinc cation only in monodentate fashion. These two possibilities, namely bidentate as contrasted with monodentate coordination, are indicated by structures MO−Zn-2 (bidentate) and MO−Zn-1 (monodentate). For simplicity, other ligands such as acetone required to complete the coordination of zinc are omitted from Scheme 5.

Previous NMR studies of related MO systems, typically at low temperatures (−22 to −45 °C), have emphasized the significance of the TTC and CTC transoid isomers relative to the TTT and CTT forms.[19] Clearly, if these are the favored MO forms, formation of the monodentate Zn complex, MO−Zn-1, should be favored kinetically over the MO−Zn-2 bidentate complex. Higher concentrations of CTC/TTC would enhance the rate of formation of MO−Zn-1, whose structure only involves complexation of the single aryloxide-type O-center with

TABLE 1: Approximate First-Order Half Lives for MO Systems with Zinc and Comparison to the Half Life without Zinc

f^a	$[Zn]_{total}$, mM	k_{app}, s^{-1} [b]	$t_{1/2}$, min	ratio[c]
0.5	0.037	5.01×10^{-4}	23	2.1
1.0	0.074	3.01×10^{-4}	38	3.3
5.0	0.36	1.94×10^{-4}	59	8.5
10	0.69	1.92×10^{-4}	60	8.6
50	3.6	1.20×10^{-4}	96	13.7

[a] Ratio of the concentration of added $Zn(ClO_4)_2$ to concentration of MO (SO). [b] Apparent first-order rate constants determined for the linear portion of the MO−Zn reversion curve. [c] Ratio of the approximate first-order half-life, $t_{1/2}$, for MO−Zn, as compared to the $t_{1/2}$ for MO (i.e., in the absence of zinc), 7.0 min; ratio = $t_{1/2}$(MO−Zn)/$t_{1/2}$ (MO no zinc).

zinc. However, a more recent NMR study of the MO forms obtained from the SO, 5′-hydroxy-1,3,3-trimethylspiro(indolino-2,3′-[3*H*]naphtho[1,2-*b*]-[1,4]oxazine), which differs from the SO of our study only in that the 5′ position (ortho to the O−C bond of the spirooxazine) is substituted with an OH group, identified all four transoid isomeric MO forms. The equilibrium mixture (−30 °C, $CDCl_3$) consisted of TTC (69%), TTT (17%), CTT (8%), and CTC (6%); the TTC and TTT forms were favored. It should be noted that the 5′ hydroxyl group is presumably H-bonded to the aryloxide oxygen, a feature nonexistent in our MO, whereas TTC should lead to the monodentate MO−Zn-1 and TTT is the reasonable precursor of the bidentate zinc complex, MO−Zn-2 (Scheme 5). It might be argued that *both* mono- and bidentate complexes could be involved in the kinetics of reversion of MO to SO here. It is noteworthy that, in a preliminary communication, complexation of the open form of a related spiroquinoxazine was shown to occur to give bidentate and monodentate forms comparable to MO−Zn-2 and MO−Zn-1, respectively.[20]

However, as will be shown, analysis of the UV−vis spectra (Section 2) argues in favor of the presence of *a single kinetically active MO−Zn complex*. This study does not permit us to differentiate between the zinc complexes presented, or other possible structures not shown.

The present results allow determination of the enhancement of MO lifetime in the SO−MO system afforded by zinc complexation. Comparing Figures 2 and 3, it is apparent, qualitatively, that zinc acts to enhance MO lifetime substantially. Approximate first-order half-lives for reversion of MO−Zn to SO (Table 1) will be discussed below.

2. Deconvolution of UV−vis Spectra of MO−Zn Complex(es). Statistical analysis (principal component analysis, PCA)[21] of the spectrum at various stages of thermal reversion of MO to SO without zinc (Figure 2) showed that there was only one species absorbing in the 400−700 nm region. Sequential spectra recorded at comparable stages of reaction in the presence of progressively larger $Zn(ClO_4)_2$ concentrations are shown in Figure 3. The spectrum recorded without zinc is labeled $j = 1$ for purposes of discussion, and $j = 2$ corresponds to a zinc/MO ratio of 1:1 and so forth, up to $j = 5$ (zinc/MO ratio of 50:1). PCA performed (see Supporting Information, S1) on the four spectra with different concentrations of zinc present (i.e., $j > 1$) indicated that there were only two species absorbing in this region. The eigenvalues of the correlation matrix[21] are 3.78, 0.21, 0.01, and 0, which would normally indicate that only one component, that is, that with the 3.78 eigenvalue, was meaningful. Because free MO and the complex (MO−Zn) have a considerable degree of overlap in their spectra, the eigenvalue 0.21 is deemed significant and was included in the analysis.

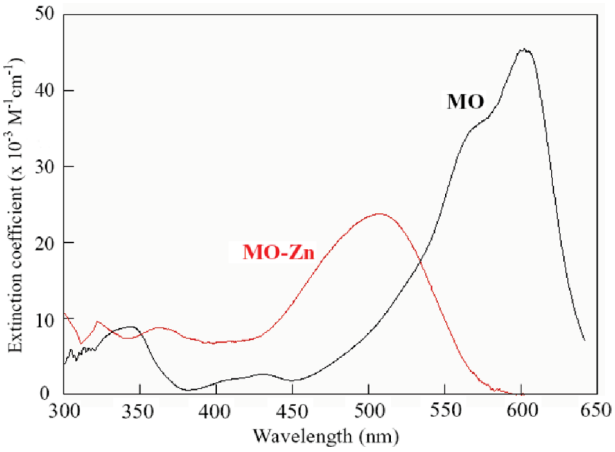

Figure 4. Comparative spectra showing the deconvoluted MO−Zn (520, 365 nm) and MO bands (605, 570 shoulder) recorded at ca. 250 s. Extinction coefficients $\varepsilon(\lambda)$ in M^{-1} cm^{-1}. The absorption around 345 nm appears also in the spectrum of SO.

Subtraction of spectrum 1 (the spectrum of MO in the absence of zinc, $j = 1$) multiplied by a suitable constant, c_j, was equal to the ratio of the measured absorbances at 615 nm, which fell in the middle of the region in which this ratio was nearly constant, indicating that MO−Zn was not contributing to the absorption. Thus, the extinction coefficient of MO−Zn at 605 nm was found to be close to zero.

To establish magnitudes of the extinction coefficients, the known value of the extinction coefficient of MO at 605 nm (obtained from spectra where SO was irradiated to give MO in the absence of zinc) was used, 45 240 M^{-1} cm^{-1}, as determined from the kinetics in the absence of zinc (*vide infra*), together with the measured absorbances at 520, 536, and 605 nm. An apparent isosbestic point at 536 nm, suggests that [MO] + [MO−Zn] = b_0. Since the total concentration, b_0, is imperfectly controlled, assumed small concentration differences were corrected by scaling the spectra to set the absorbance at 536 nm equal to 0.879 for all.

With no zinc ($j = 1$; $A_j = A_1$):

$A_{1,605} = \epsilon_{b,605} b_0$

$A_{1,520} = \epsilon_{b,520} b_0$

With zinc present ($j > 1$):

$A_{j,605} = \epsilon_{b,605}$[MO]

$A_{j,520} = \epsilon_{b,520}$[MO] + $\epsilon_{c,520}$[MO−Zn]

Whence:

$\epsilon_{c,520} = \epsilon_{b,605} (A_{j,520}A_{1,605} - A_{1,520}A_{j,605})/A_{1,605}(A_{1,605} - A_{j,605})$.

The mean of three values from this analysis was 23 800 ± 300 M^{-1} cm^{-1} for the 520 nm peak assigned to the MO−Zn complex. The uncertainty in this extinction coefficient was assumed to apply to the other extinction coefficients. The spectrum derived was rescaled to set the extinction coefficient at 520 nm equal to the above value, such that ϵ_{max} = 25 040 M^{-1} cm^{-1}, at 508 nm. The derived spectrum of MO−Zn is shown in Figure 4 and shows the major band at 520 with a small peak at 365 nm; the latter MO−Zn peak is obscured in the combined MO + MO−Zn spectrum.

The salient point of this analysis is that only a single MO−Zn species is detectable by UV−vis spectroscopy at −30 °C. Either only one MO−Zn form is present in the system or the MO−Zn complexes are in rapid equilibrium. Major structural/electronic reorganization is expected to be involved in going from the monodentate MO−Zn-1 to the bidentate MO−Zn-2 isomer (and vice versa), presumably preceding through the various MO transoid structures (i.e., TTC, CTC, CTT, TTT; Scheme 5). On this basis, we favor the first explanation: the presence of *a single kinetically active* MO−Zn species.

3. Mechanism and Kinetics. An overview of the SO−MO kinetic processes involved, both with and without zinc, may be gleaned from concentration versus time graphs for all relevant species. Thus, deconvolution of spectra permitted calculation of concentrations of MO and MO−Zn, and that of SO by difference, as functions of time, both during irradiation and afterward. Figure 5 shows concentration (μmol L^{-1}) of all species—i.e., SO, MO, and, where pertinent, MO−Zn—plotted against time (ks). In each, the time at which the UV lamp was turned off is apparent from the sharp break in the curve of [SO] versus time, at ca. 0.3 ks. Turning to Figure 5a, where no zinc is present ($f = 0$), irradiation of SO for ca. 300 s leads to an approximately photostationary concentration of the open form (i.e., [X] = [MO]) and the concentration of the closed form, SO, is at a minimum. Thermal reversion of MO to SO follows an exponential decay curve where MO has essentially all reverted by about 3 ks. Addition of less than equimolar zinc (as $Zn(ClO_4)_2$; $f = 0.5$, the ratio of $Zn(ClO_4)_2$/MO in Figure 5b) results in the appearance of a new species, MO−Zn (as shown in the separate deconvolution experiments, above), upon similar irradiation of SO. Free MO is the dominant product and again undergoes exponential reversion to MO, whereas MO−Zn reverts to SO in apparent linear decay. Neither MO nor MO−Zn species have undergone ring closure to SO to the extent of indetectability until 4 ks. This suggests that the presence of zinc, *even at less than equimolar ratio*, enhances the lifetime of the ring-open species.

Under equimolar conditions ($f = 1.0$; Figure 5c) a crossover of the MO and MO−Zn reversion curves can be discerned at about 1.5 ks. Although free MO is still dominant, it is clear that the first order ring closure of MO results in a shorter lifetime for it compared to MO−Zn. Complexation of MO by zinc leads to an expanded lifetime for MO−Zn. Similar considerations apply to Figure 5d, where zinc is in excess ($f = 5$), and the crossover of decay curves for MO and MO−Zn occurs earlier (ca. 0.5 ks) and to Figure 5e ($f = 10$), where crossover occurs earlier still.

With a large excess of zinc ($f = 50$; Figure 5f) irradiation of SO now gives MO−Zn as the dominant species, although free MO concentration is still appreciable. Notable in the plot is the fact that MO−Zn concentration continues to rise even after irradiation of SO to form MO has ceased, emphasizing the interconvertibility of MO species. Nonetheless, MO and MO−Zn revert to SO as before, but at 4 ks neither has disappeared.

The mechanism of ring-opening and complexation with zinc reasonably consists of four steps, namely, (1) photogeneration of MO from SO (k_1), (2) thermal reversion of SO (k_2), (3) reaction of MO with zinc species to form the complex MO−Zn (k_3), and (4) the dissociation of MO−Zn (k_4). As a first approximation the zinc species are given simply as zinc ion in the reactions and equations below, although further kinetic analysis proved that the species involved in acetone at −30 °C are more complex.

$$\mathrm{SO} \xrightarrow{k_1,\, h\nu} \mathrm{MO\ (during\ irradiation\ only)} \qquad (1)$$

Equation 1 represents photogeneration of MO, where the rate constant, k_1, depends upon quantum yield (Φ) at the wavelength of irradiation (319 nm) and the intensity (I) of incident light. The intensity as determined by ferrioxalate actinometry before

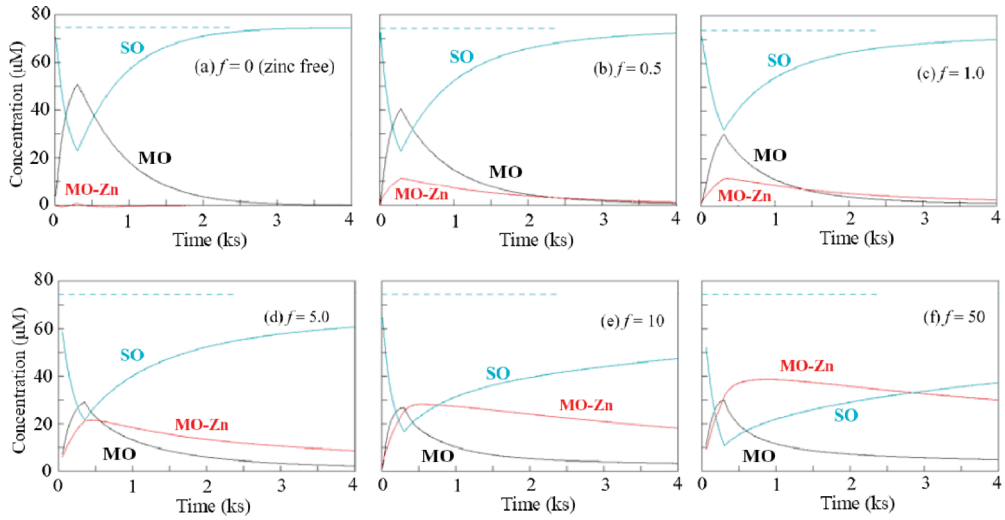

Figure 5. Photogeneration of MO from SO and reversion, with and without zinc, in acetone at −30 °C. Concentrations in μM; [X] = [SO] (green), [MO] (black), and [MO−Zn] (red) versus time in ks. The traces (a−f) correspond to increasing ratios of added zinc relative to [SO], 0, 0.5, 1, 5, 10, and 50 to 1, respectively. In each, [MO] reaches a maximum and [SO] a minimum at ca. 0.3 ks, at which time irradiation ceased.

and after each run was constant. However, uncertainties arise that limit the precision of the k_1 value reported which, nonetheless, served as a useful input value in the more complex curve-fitting required to extract rate constants k_3 and k_4 (vide infra).

$$\mathrm{MO} \xrightarrow{k_2} \mathrm{SO} \tag{2}$$

$$\mathrm{MO} + \mathrm{Zn}^{2+} \xrightarrow{k_3} \mathrm{MO} - \mathrm{Zn}^{2+} \tag{3}$$

$$\mathrm{MO} - \mathrm{Zn}^{2+} \xrightarrow{k_4} \mathrm{MO} + \mathrm{Zn}^{2+} \tag{4}$$

The rate equations follow:

$$\frac{\mathrm{d}}{\mathrm{d}t}[\mathrm{MO}] = k_1[\mathrm{SO}] - k_2[\mathrm{MO}] - k_3[\mathrm{MO}]]\mathrm{Zn}^{2+}] + k_4[\mathrm{MO} - \mathrm{Zn}^{2+}] \tag{5}$$

$$\frac{\mathrm{d}}{\mathrm{d}t}[\mathrm{MO} - \mathrm{Zn}^{2+}] = k_3[\mathrm{MO}][\mathrm{Zn}^{2+}] - k_4[\mathrm{MO} - \mathrm{Zn}^{2+}] \tag{6}$$

a. Kinetics in the Absence of Zinc. When the concentration of zinc ion is zero (Scheme 1), eq 6 is not relevant to the analysis, the last two terms in eq 5 may be omitted, and eq 5 collapses to eq 7:

$$\frac{\mathrm{d}[\mathrm{MO}]}{\mathrm{d}t} = k_1[\mathrm{SO}] - k_2[\mathrm{MO}] \tag{7}$$

The measured absorbances at 605, 570, and 520 nm, which are related to the concentration of MO, varied with time in close proportionality to one other.

A nonlinear least-squares program (QBasic) was used to fit the curves of absorbance versus time calculated at 520 and 605 nm during irradiation. Best-fitting values for four parameters were sought: the two rate constants k_1 and k_2, and two extinction coefficients, for MO at 520 and at 605 nm. This "self-consistent" method gave $k_1 \approx 6 \times 10^{-3}$ s^{-1}, $k_2 = 1.71 \times 10^{-3}$ s^{-1}, and for the extinction coefficients, $\varepsilon(605) = 45\,240$ and $\varepsilon(520) = 13\,200$ M^{-1} cm^{-1}.

When the lamp is off (after $t \sim 300$ s), the intensity I, and consequently k_1, is zero, the first term in eq 5 may also be neglected and eq 5 transforms into eq 8, a standard first-order kinetic rate law:

$$\frac{\mathrm{d}[\mathrm{MO}]}{\mathrm{d}t} = -k_2[\mathrm{MO}] \tag{8}$$

The first order plots (not shown) of ln(A_λ) versus t (for each λ = 520, 570, and 605 nm) yielded good straight lines ($r^2 \geq 0.99$) with negative slopes (k_2) of magnitude (1.628 ± 0.009) × 10 $^{-3}$ s^{-1}, in fair agreement with the value determined from the fitting program (eq 7). A further test of the robustness of the values of these constants (see Supporting Information, S2) led us to report as our best values, with estimated uncertainties: $k_1 = (5.7 \pm 0.3) \times 10^{-3}$ s^{-1}; $k_2 = (1.7 \pm 0.1) \times 10^{-3}$ s^{-1}. Delbaere and co-workers[19a] reported a value of 3.31 × 10^{-3} s^{-1} for k_2 at −30 °C in CD_3CN determined by ^{1}H NMR, while the comparable rate constant extrapolated from the Arrhenius plot of Chu[22] for reversion of MO to SO in ethanol at −30 °C is ca. 6 × 10^{-4} s^{-1}. Therefore, k_2 determined in the current study is a reasonable value at this temperature in an aprotic polar solvent like acetone.

The first-order half-life ($t_{1/2}$) of the open MO form, in the absence of zinc, can be calculated directly from k_2 as 407 s (7.0 min), a measure of the relative ease of ring closure back to the spirocyclic SO. The effect of zinc on $t_{1/2}$ will be discussed below.

b. Kinetics When Zinc Is Present. The mechanism is now represented by Schemes 4 and 5, detailed by eqs 3−6.

However, it is necessary to consider the state of $Zn(ClO_4)_2$ in acetone. This has been studied by conductance, along with the perchlorates of divalent manganese, cobalt, nickel, and copper, by Grzybkowski and Pilarzyk (25 °C)[23] and involves coordination of the metal ion by solvent and association with perchlorate. The implications will be discussed below. As a first

assumption for kinetic analysis, complete dissociation was posited, that is, the available zinc ion concentration was taken to be equal to the total $Zn(ClO_4)_2$ concentration. Determination of the remaining rate constants k_3 and k_4 required numerical integration of eqs 5 and 6 simultaneously, seeking best values for the constants by a nonlinear least-squares procedure at each metal:substrate ratio, designated f for the kinetic analyses. Values of four extinction coefficients (see Deconvolution, above) and the rate constants k_1 and k_2 (from the zinc-free analysis) were treated as inputs. Fits to the absorbance data (not shown) were quite poor, as could be expected from the more complex nature of $Zn(ClO_4)_2$ in acetone.[23]

In the Grzybkowski and Pilarzyk study[23] the divalent transition metal cations, M^{2+}, examined were concluded to exist as hexacoordinate complexes with acetone. By the Fuoss−Edelson analysis, an equilibrium constant for association of $M(acetone)_6^{2+}$ *as a group* with a single perchlorate counterion was determined as $(8 \pm 3) \times 10^3$ M^{-1}; conductance data for all of the metal perchlorates were similar, falling within narrow boundaries set by copper(II) and nickel(II) perchlorates. The same approach applied to $Zn(ClO_4)_2$ in acetonitrile at −30 °C yielded a first association constant of 34 M^{-1}. Importantly, in this work by Petrucci and co-workers,[24] the value for the same constant at 25 °C was reported as 48 M^{-1}, that is, only a factor of 1.4 larger. By another approach estimates for both a first and a second association equilibrium constant were obtained by Grzybkowski and Pilarzyk.[23] The first perchlorate association constant was estimated to be 1.1×10^4 and the constant for association with a second perchlorate was found to be 5.0×10^2 M^{-1}. Assuming that the 1.4 temperature factor found for zinc association with one perchlorate *in acetonitrile* equally applies to both association constants *in acetone*, then approximate association constants at −30 °C can be proposed: 7.9×10^3 (1st association) and 3.6×10^2 M^{-1} (2nd association). These constants are the reciprocal of the dissociation constants that are germane to the present kinetic analysis (cf. eq 9 and 10 below), that is, values of $K_1 \approx 3 \times 10^{-3}$ and $K_2 \approx 1 \times 10^{-4}$ M dissociation constants are estimated from the association constant data.[23,24]

The assumption that $Zn(ClO_4)_2$ is ion-paired in acetone at −30 °C requires two equilibrium steps, and the dissociation of $Zn(ClO_4)_2$ can be represented by (where all species are solvated by acetone):

$$Zn(ClO_4)_2 = ZnClO_4^+ + ClO_4^-; K_1 \quad (9)$$

$$ZnClO_4^+ = Zn^{2+} + ClO_4^-; K_2 \quad (10)$$

In this case, kinetic analysis involves fitting the absorbance data seeking best values for the remaining two rate constants, (k_3, k_4) plus the two dissociation constants for the salt. The estimates for k_3 and k_4 (from the first trial fitting) were also used as initial input values, along with k_1 and k_2, to be refined in the fitting process (see Supporting Information, S2, Tables ST1, ST2).

Proceeding to the "rising portions" of the concentration versus time plots (Figure 5; $t = 0$ to ca. 0.3 ks), when the sample was undergoing irradiation, fitting yielded the following rate constants: $k_1 = (5.0 \pm 1.2) \times 10^{-3}$ s^{-1}, $k_2 = (1.9 \pm 0.9) \times 10^{-3}$ s^{-1}, $k_3 = 106 \pm 12$ M^{-1} s^{-1}, and $k_4 = 155 \pm 40$ s^{-1}. These values were obtained from fitting at each concentration ratio of zinc from $f = 0$ (where only k_1 and k_2 are relevant) to $f = 50$. No trends in the rate constant values as a function of zinc concentration were noted (Tables ST1 and ST2). Note that the values of k_1 and k_2 in this early portion of the process are not significantly perturbed from the same values determined without zinc. However, the larger uncertainties inherent in the k_1 determination in the absence of zinc still apply.

Step-wise equilibrium constants for dissociation of $Zn(ClO_4)_2$ were determined in the same fit of the rising portion of the concentration versus time plots. These exhibited significantly larger errors than the rate constants and mean values are: $K_1 \approx 6 \times 10^{-3}$ M and $K_2 \approx 4 \times 10^{-7}$ M. The magnitude of the errors is emphasized when the "reversion portions" of the concentration time plots (Figure 5, t ca. 0.3−4 ks) are similarly fitted. It is noteworthy that K_1 determined here is within an order of magnitude of the value estimated[23] corrected for temperature,[24] that is, here $K_1 \approx 6 \times 10^{-3}$ as compared to the estimated $K_1 \approx 3 \times 10^{-3}$ M. The value of K_2, however, is significantly different from that estimated, that is, $K_2 \approx 4 \times 10^{-7}$ M versus the estimated value $K_2 \approx 1 \times 10^{-4}$ M.

In the reversion portion of the concentration−time trace (Figure 5, t = ca. 0.3−4 ks) irradiation of SO has ceased; k_1, the rate constant for this photogeneration step, is irrelevant. The fit to the concentration−time graph gave values of rate constants as: $k_2 = 1.46 \pm 0.26 \times 10^{-3}$ s^{-1}, $k_3 = 260 \pm 155$ M^{-1} s^{-1}, and $k_4 = 119 \pm 5$ s^{-1}. The stepwise $Zn(ClO_4)_2$ dissociation constants in acetone from this fit have values of $4.5 \pm 2.4 \times 10^{-5}$ (K_1) and $9 \pm 5 \times 10^{-10}$ M (K_2).

Comparison may be made to the limited literature data concerning the effect of transition M^{n+} on the kinetics of reversion of MO forms. Kim et al. thus found rate constants for reversion of the MO considered here between 3.96×10^{-2} and 5.40×10^{-2} s^{-1} in the presence of varying concentrations of $Zn(NO_3)_2$, while somewhat lower values for this rate constant were reported when zinc 2-hydroxybenzoate was used as the zinc source.[25] The faster rate of reversion found in these systems may arise from interplay of a range of factors including differences in dissociation of the zinc salts used or in differences in temperature or solvent. A series of 5′-(benzotriazol-2-yl)spiroindolinonaphthoxazines were examined by Jeliazkova and co-workers,[26] who found that the rate constant for photogeneration of MO in the presence of Ni(II), Co(II), and Zn(II) nitrates in acetone (20−50 °C) was ca. 1×10^{-3} s^{-1} for all systems. This approximate rate constant is in reasonable agreement with k_1 in our study in the presence of zinc, given the structural and temperature difference involved in the comparison.

Treating the concentration versus time data (Figure 5) as though all data fit first-order kinetics, that is, replotting the data as $\ln([SO]/[SO]_0 - 1)$ versus time, yields traces where an approximately linear region emerges (see Supporting Information graphs, SG1−SG6); the data follow first order treatment for these data regions. Note that $[SO]_t$ is calculated from $[SO]_0 - [MO] - [MO{-}Zn] = [SO]$ at a given time t; values of [MO] and [MO−Zn] derive from deconvoluted spectra. From these regions apparent first order rate constants (k_{app}) can be determined and the corresponding half-lives calculated (Table 1).

As can be seen (Table 1), even a 0.5 ratio of added zinc to the system results in a significant increase in the lifetime of MO, that is, the ratio of $t_{1/2}$ here to that in the system sans zinc is 2.1. This factor increases with increasing amounts of $Zn(ClO_4)_2$ until at a ratio of 50:1 ($f = 50$), the enhancement of the lifetime, according to this ratio, is greater than 13.

Clearly, the presence of divalent zinc provides a route to the stabilization of the open form of MO, enhancing the bistability of this potential photoswitch.

CHART 1: Comparisons of the Activation Barriers for Reversion and between the MO and Related MC Systems

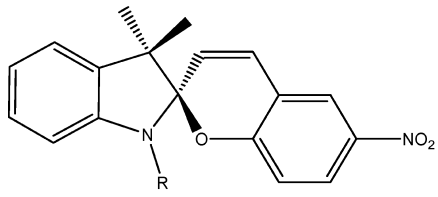

SP:

1a R=CH_3
1b R=$(CH_2)_2COOH$
1c R=$(CH_2)_4COOH$
1d R=$(CH_2)5COOH$

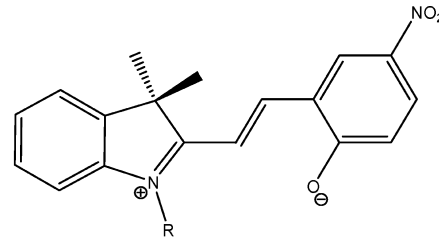

MC:

2a R=CH_3
2b R=$(CH_2)_2COOH$
2c R=$(CH_2)_4COOH$
2d R=$(CH_2)_5COOH$

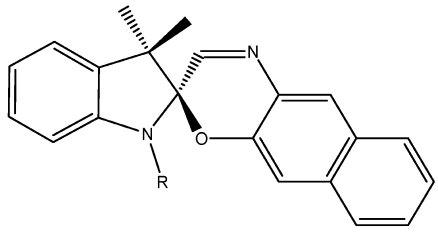

SO:

3a R=CH_3

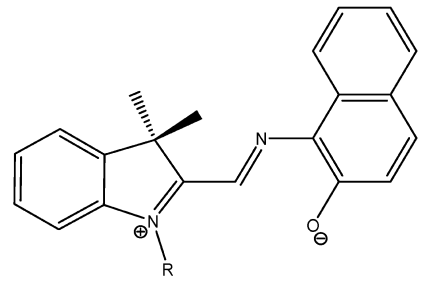

MO:

4a R=CH_3

TABLE 2: Free Energies of Activation ($\Delta G^{\ddagger}$) for Selected MO and MC for Thermal Reversion to the Respective Closed Forms

system	Zn	rate constant, s^{-1} mol^{-1}	$\Delta G^{\ddagger}$, kJ	ref
4a, acetone, 243 K		$k_2 = 1.7 \times 10^{-3}$	62.0	This work
4a, ethanol, 273 K		$k = 2.67 \times 10^{-2}$	74.9	22
2a, acetone, 298 K		$k = 7.3 \times 10^{-3}$	85.2	28
2b, acetone, 298 K		$k = 2.28 \times 10^{-2}$	82.4	9
2c, acetone, 298K		$k = 1.13 \times 10^{-3}$	89.8	9
2d, acetone, 298 K		$k = 2.99 \times 10^{-3}$	87.4	9
4a, acetone, 243 K	$f = 1$	$k_{app} = 5.01 \times 10^{-4}$	74.5	This work
4a, acetone, 243 K	$f = 50$	$k_{app} = 1.20 \times 10^{-4}$	77.3	This work

4. Energetics of MO Reversion: Comparison to MC Systems. Conversion of the relevant rate constants to Gibbs free energies of activation ($\Delta G^{\ddagger}$) permits comparisons of the activation barriers for reversion and, more importantly, between the MO and related merocyanine (MC) systems (Chart 1). The $\Delta G^{\ddagger}$ values were calculated via the Eyring equation[27] from reported rate constant data for a given temperature; $\Delta G^{\ddagger}$ values, rate constants for ring closure from the open to the respective closed forms, and the temperature of the kinetic measurement are collected in Table 2.

As can be seen from Table 2, MO reversion to SO (**4a** → **3a**) is typically more facile than a common MC to SP reversion (**2a** → **1a**), that is, $\Delta G^{\ddagger}$ for **4a** = 62.0 kJ mol^{-1}, whereas $\Delta G^{\ddagger}$ for the **2a** is 85.2 kJ mol^{-1}. Note that the stabilizing effect of the 6-nitro group on the MC form, **2a** (6-nitro-BIPS, Scheme 1), may be significantly greater than that of the fused benzene ring on **4a** studied here. To our knowledge, kinetic studies involving the nitro-substituted spirooxazine analogue of **2a** have not been reported.

Comment may also be made on the role of solvent. Comparison of the activation barrier, $\Delta G^{\ddagger}$, determined from the 273 K reversion rate constant for **4a** reported by Chu in ethanol ($\Delta G^{\ddagger}$ = 74.9 kJ mol^{-1}) to that based on the 243 K reversion k_2 measured here in acetone ($\Delta G^{\ddagger}$ = 62.0 kJ mol^{-1} for **4a**), suggests that the dipolar resonance forms contribute significantly to **4a** stability; the more polar protic ethanol stabilizes MO better than aprotic acetone does. Further work involving a range of solvents would be required to confirm this surmise, as we have reported for **2a** and related MC systems.[28]

The efficacy of zinc in stabilizing **4a** is apparent in comparison of $\Delta G^{\ddagger}$ (acetone) without zinc (62.0 kJ mol^{-1}) and with equimolar zinc ($f = 1$, 74.5 kJ mol^{-1}). The latter value is based on k_{app} for reversion (Table 1). For SP−MC systems where R attached to N of the spiroindolino ring comprises a methylenic chain ending in a carboxylic acid (i.e., $(CH_2)_nCOOH$, $n = 2$, 4, 5; **2b**−**2d**) the UV−vis spectra showed no band ascribable to free MC when the corresponding SP (i.e., **1b**−**1d**) was irradiated in the presence of equimolar $Zn(ClO_4)_2$. In these cases even equimolar zinc chelates the open MC fully. In contrast, the related experiments with MO, **4a**, yielded spectra where both free MO and MO−Zn were present and kinetic analysis required deconvolution of these spectra (vide supra). Clearly, when using purpose-built MC, such as **2b**−**2d**, to chelate zinc, complexation is complete and the resultant stabilization of the MC form maximized.

At higher molar ratios of added zinc $\Delta G^{\ddagger}$ for reversion of MO, **4a**, rises ($f = 50$, Table 2) to a value of 77.3 kJ mol^{-1}, more nearly approaching that of the standard MC, **2a** (85.2 kJ mol^{-1}).

Further exploitation of divalent metal ion stabilization of the MO should arise from the use of stabilizing solvents (ethanol vs acetone) and from understanding of the nature of zinc complexation in MO−Zn (i.e., MO−Zn-1 vs MO−Zn-2).

TABLE 3: Compositions of Solutions[a]

run No.	factor (nominal Zn ion/SO ratio)	vol. of 4.55×10^{-3} M SO, μL	vol. of 9.1×10^{-3} M $Zn(ClO_4)$, μL	resultant concentration (μM)of SO	resultant concentration (μM)of Zn(II)	delay, s (approx)
1	0	50	0	74.6	0	12
2	0.5	50	12.5	74.3	37.1	0
3	1.0	50	25	74.0	74.0	0
4	5	50	125	71.7	358	36
5	10	50	250	69	690	0
6	50	50	125*	72	3600	30

[a] Stock solution of zinc salt was 9.1×10^{-2} M.

Conclusions

This work on MO → SO reversion kinetics in the absence/presence of zinc has shown:

(1) MO reverts at −30 °C in acetone to the colorless SO form with a rate constant, $k_2 = 1.65 \times 10^{-3}$ s^{-1} in the absence of added zinc (a half-life for MO of 7 min).

(2) Addition of $Zn(ClO_4)_2$ leads to formation of MO−Zn complex, whose spectroscopic features were determined by deconvolution of spectra of the complex and free MO. MO−Zn has $\lambda_{max} = 520$ nm, $\varepsilon_{max} = 23\,800$ M^{-1} cm^{-1}.

(3) Intervention of the MO−Zn complex substantially enhances the lifetime of MO, as described by concentration versus time graphs (Figure 5). Approximate first−order kinetics (Table 1) shows that at a ratio (f) of $Zn(ClO_4)_2$: MO of 50: 1, $t_{1/2} = 96$ min, > 13-fold enhancement in lifetime relative to MO without zinc.

(4) For the first time, to our knowledge, microscopic rate constants (k_1, k_2, k_3, and k_4) and equilibrium constants ($K_1$and K_2) have been extracted via curve-fitting.

(5) Althouth kinetics does not reveal the exact nature of MO−Zn (e.g., MO−Zn-1 vs MO−Zn-2), nor the precursor isomers of MO (CTC, etc.), preliminary results of a DFT calculational study[29] shed light on the structures and relative stability of these essential intermediates. Further calculational work, including simulation of UV−visible spectra, is in progress to ascertain the structure(s) of MO−Zn and rank the structures in order of energetics, elucidating the pathways of formation of MO−Zn-1 (monodentate) and MO−Zn-2 (bidentate) complexes and the involvement of TTC or other conformers (Scheme 5).

Overall, the study points the way to the use of divalent transition metal ions in the development of bistable photochemical switches.

Experimental Section

Instrumentation. ^{1}H and ^{13}C NMR spectra were recorded on a Bruker Avance-300 or Avance-400 (operating at 300 and 400 MHz for proton NMR, automatic sample changer, BB autotuning) spectrometer. Mass spectroscopic analysis was performed using electron impact (EI), chemical ionization (CI), and electrospray ionization (ESI), as warranted. Melting points (uncorrected) were measured using a Fisher-Johns melting point apparatus.

The photochemical experiments used a S2000 miniature fiber optic spectrophotometer (Ocean Optics, Dunedin, FL) connected to a four-way temperature-controlled cuvette holder (Quantum Northwest, Spokane, WA) via 400 μm optical fibres to measure absorbance. The irradiation source was a 200 W Hg/Xe lamp attached to a model 101 0.2 m f/4 monochromator equipped with a 1200 g mm^{-1}, 300 nm blaze standard grating (Photon Technology International) connected to the cuvette holder via a 10 mm quartz fiber bundle. Data were collected with 011 Base 32 software. The light intensity of the Hg/Xe irradiation source was measured by ferrioxalate actinometry[30] and was found to be stable from day to day.

Preparation of SO. Starting materials and inorganic reagents for the preparation of SO were procured in highest purity available and were used without further purification. Reagent grade or higher purity solvents were used as purchased.

Spirooxazine (SO) was prepared through the reaction of 1-nitroso-2-naphthol with 1,3,3-trimethyl-2-methyleneindoline (Fischer base, freshly distilled), following the method of Chu,[22] mp 122−124 °C (lit.[22] 124−125 °C). ^{1}H NMR and ^{13}C NMR (δ rel. to TMS) gave spectroscopic data in reasonable agreement with that reported by Zaichenko et al.[31] TOF-MS (ESI) (high res.): $M^+ = 328.1583$ (calc. 328.1576 for $C_{22}H_{20}N_2O$). Tlc (single spot): rf. 0.69 (benzene), 0.50 (80:20 benzene/hexane).

Kinetic Measurements. Solutions were prepared by adding 3 mL of acetone to the volumes of $Zn(ClO_4)_2$ solutions in acetone shown in Table 3, under dry nitrogen, in a 1 cm path cuvette. The cuvette was placed in the constant-temperature enclosure, maintained at −30 °C and equipped with magnetic stirrer. The spectrum was scanned to provide a blank. After addition of the volume of SO solution (Table 3), the solution was irradiated at 319 nm while the absorption spectrum was repeatedly scanned. The full spectrum from 300 to 800 nm was recorded every 250 s starting at 300 s. The absorbance values at 520, 570, and 605 nm were recorded every 5 s from the start. The UV lamp was turned on, and the scan begun immediately, or after a short delay as noted in the Table. At approximately 300 s the lamp was turned off, and the scanning continued as before until about 5000 s elapsed time.

Acknowledgment. We acknowledge funding by the Natural Sciences and Engineering Research Council of Canada (E. B.), and Grenfell Campus, Memorial University of Newfoundland Vice-President's Research Fund (J. M. D.). Helpful discussions with Dr. Yong Park and Prof. J.-M. Nunzi (Queen's) are gratefully acknowledged.

Supporting Information Available: Notes on deconvolution (S1), fitting of kinetic constants (S2), Tables of constants at various concentration ratios of $Zn(ClO_4)_2$ to SO (Tables ST1 and ST2), approximate first order plots for reversion of MO to SO (Graphs SG1−SG6). This material is available free of charge via the Internet at http://pubs.acs.org.

References and Notes

(1) (a) Crano, J. C., Guglielmetti, R. J., Eds.; *Organic Photochromic and Thermochromic Compounds*; Topics in Applied Chemistry; Kluwer Academic/Plenum: New York, 1999; Vols. 1 and 2. (b) Dürr, H., Bouas-Laurent, H., Eds. *Photochromism, Molecules and Systems in Studies in Organic Chemistry*; Elsevier: Amsterdam, 1990; Vol. 40.

(2) Hirschberg, Y. *J. Am. Chem. Soc.* **1956**, *78*, 2304–2312.

(3) (a) Berkovic, G.; Krongauz, V.; Weiss, V. *Chem. Rev.* **2000**, *100*, 1741–1754. (b) Kawata, S.; Kawata, Y. *Chem. Rev.* **2000**, *100*, 1777–1788. (c) Irie, M. *Chem. Rev.* **2000**, *100*, 1630.

(4) Wojtyk, J. T. C.; Kazmaier, P. M.; Buncel, E. *J. Chem. Soc., Chem. Commun.* **1998**, 1703–1704.

(5) Wojtyk, J. T. C.; Wasey, A.; Kazmaier, P. M.; Hoz, S.; Buncel, E. *J. Phys. Chem. A.* **2000**, *104*, 9046–9055.

(6) (a) Feringa, B. L.; Lager, W. F.; DeLange, B. *Tetrahedron* **1993**, *49*, 8267–8310. (b) Parthenopoulos, D. A.; Rentzepis, P. M. *Science* **1989**, *245*, 843–845. (c) Piyaket, R.; Cokgor, I.; McCormick, F. B.; Esener, S.; Dvornikov, A. S.; Rentzepis, P. M. *Opt. Lett.* **1996**, *14*, 1032–1034. (d) Dvornikov, A. S.; Walker, E. P.; Rentzepis, P. M. *J. Phys. Chem. A.* **2009**, *113*, 13633–13644.

(7) (a) Piantik, M.; Schulze, G.; Koch, M.; Franke, K. J.; Leyssner, F.; Kruger, A.; Navia, C.; Miguel, J.; Bernien, M.; Wolf, M.; Kuch, W.; Tegeder, P.; Pascual, J. I. *J. Am. Chem. Soc.* **2009**, *131*, 12729–12735. (b) Muhlstein, L. A.; Sauer, J.; Bein, T. *Adv. Funct. Mater.* **2009**, *920*, 332–341. (c) Rosario, R.; Gust, D.; Hayes, M.; Springer, J.; Garcia, A. A. *Langmuir* **2003**, *19*, 8801–8806. (d) Suzuki, T.; Lin, F. T.; Priyadashy, S.; Weber, S. G. *Chem. Commun.* **1998**, *24*, 2685–2686.

(8) (a) Xiao, N. N.; Chen, Y.; Lemieux, R.; Buncel, E.; Iftime, G.; Kazmaier, P. M. *Mol. Cryst. Liq. Cryst.* **2005**, *431*, 337–344. (b) Wojtyk, J. T. C.; Wasey, A.; Xiao, N. N.; Kazmaier, P. M.; Hoz, S.; Yu, C.; Lemieux, R. P.; Buncel, E. *J. Phys. Chem. A.* **2007**, *111*, 2511–2516.

(9) Wojtyk, J. T. C.; Kazmaier, P. M.; Buncel, E. *Chem. Mater.* **2001**, *13*, 2547–2551.

(10) Keum, S. R.; Ku, B. S.; Shin, J. T.; Ko, J. J.; Buncel, E. *Tetrahedron* **2005**, *61*, 6720–6725.

(11) Keum, S. R.; Lee, M. J.; Swansburg, S.; Buncel, E.; Lemieux, R. P. *Dyes Pigments* **1998**, *39*, 383–388.

(12) (a) Harbron, E. J.; Davis, C. M.; Campbell, J. K.; Allred, R. M.; Kovary, M. T.; Economou, N. J. *J. Phys. Chem. C* **2009**, *113*, 13707–13714. (b) Raboin, L.; Matheron, M.; Biteau, J.; Gacoin, T.; Boilot, J. P. *J. Mater. Chem.* **2008**, *18*, 3242–3248. (c) Wu, Y.; Sasaka, T.; Kazushi, K.; Seo, T.; Sakurai, K. *J. Phys. Chem. B* **2008**, *112*, 7530–7536. (d) Yee, L. H.; Hanley, T.; Evans, R. A.; Davis, T. P.; Ball, G. E. *J. Org. Chem.* **2010**, *75*, 2851–2860.

(13) Swansburg, S.; Choi, Y. K.; Keum, S. R.; Buncel, E.; Lemieux, R. P. *Liq. Cryst.* **1998**, *24*, 341–346.

(14) Whelan, J.; Wojtyk, J. T. C.; Buncel, E. *Chem. Mater.* **2008**, *20*, 3797–3799.

(15) (a) Lokshin, V.; Samat, A.; Metelitsa, A. V. *Russ. Chem. Rev.* **2002**, *71*, 893–916. (b) Bertelson, R. C. *Photochromism*; Brown, G. H., Ed.; Wiley-Interscience: New York, 1971; Ch. 3. (c) Bohne, C.; Fang, M. G.; Li, Z. J.; Liang, Y. C.; Lusztyk, J.; Scaiano, J. C. *J. Photchem. Photobiol. A: Chem.* **1992**, *66*, 79–90.

(16) (a) Nishikiori, H.; Tanaka, N.; Takagi, K.; Fujii, T. *J. Photochem. Photobiol. A: Chem.* **2007**, *189*, 46–54. (b) Nishikiori, H.; Tanaka, N.; Takagi, K.; Fujii, T. *J. Photochem. Photobiol. A: Chem.* **2006**, *183*, 53–58.

(17) (a) Lokshin, V.; Samat, A.; Metelitsa, A. V. *Russ. Chem. Rev.* **2002**, *71*, 893–916. (b) Maurel, F.; Aubard, J.; Rajzmann, M.; Guglielmetti, R.; Samat, A. *J. Chem. Soc.* **2002**, 1307–1315.

(18) Berthet, J.; Delbaere, S.; Carvalho, L. M.; Vermeersch, G.; Coelho, P. J. *Tetrahedron Lett.* **2006**, *47*, 4903–4905.

(19) (a) Delbaere, S.; Bochu, C.; Azaroual, N.; Buntinx, G.; Vermeersch, G. *J. Chem. Soc. Perkin Trans 2* **1997**, 1499–1501. (b) Berthet, J.; Delbaere, S.; Lokshin, V.; Bochu, C.; Samat, A.; Guglielmetti, R.; Vermeersch, G. *Photochem. Photobiol. Sci.* **2002**, *1*, 333–339.

(20) Preigh, M. J.; Lin, F. T.; Ismail, K. Z.; Weber, S. G. *Chem. Commun.* **1995**, 2091–2092.

(21) Johnson, D. E.; *Applied Multivariate Methods for Data Analysis*; Duxbury Press: Pacific Grove, CA, U.S.A.; 1998; Ch. 5.

(22) Chu, N. Y. C. *Can. J. Chem.* **1983**, *61*, 300–305.

(23) Grzybkowski, W.; Pilarczyk, M. *Electrochim. Acta* **1990**, *35*, 351–355.

(24) Diamond, A.; Fanelli, A.; Petrucci, S. *Inorg. Chem.* **1973**, *12*, 611–619.

(25) Kim, S. H.; Wang, S.; Ahn, C. H.; Choi, M. S. *Fibers Polymers* **2007**, *8*, 447–449.

(26) Jeliazkova, B. G.; Minkovska, S.; Deligeorgiev, T. *J. Photochem. Photobiol. A.* **2005**, *171*, 153–160.

(27) Bunnett, J. F. In *Techniques in Organic Chemistry. Rates and Mechanisms of Reactions. Part 1*; 2nd ed.; Weissberger, A., Ed.; Interscience: New York, 1961, pp 199−202.

(28) Keum, R.; Hur, M. S.; Kazmaier, P. M.; Buncel, E. *Can. J. Chem.* **1991**, *69*, 1940–1947.

(29) Buncel, E.; Stairs, R.; Dust, J.; Tian, Z.; Wyer, M.; Kraft, T.; Mosey, N. *Poster P7 presented at 10th Annual Centre for Research in Molecular Modelling Symposium*, Concordia University, Montreal, Canada, 2010.

(30) (a) Hatchard, H.; Parker, C. A. *Proc. Royal Soc. London A* **1956**, *235*, 518–529. (b) Montalti, M.; Credi, A.; Prodi, L.; Gandolfi, M. T. *Handbook of Photochemistry*, 3rd ed.; Taylor and Francis: Boca Raton, LA, U.S.A., 2006; pp 601−604.

(31) Zaichenko, N. L.; Shiyonok, A. I.; Kol'tsova, L. S.; Marevtsev, V. S. *Mol. Cryst. Liq. Cryst.* **2005**, *431*, 383–389.

JP106501E